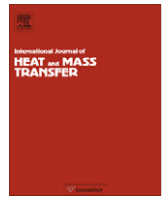




Contents lists available at ScienceDirect

International Journal of Heat and Mass Transfer

journal homepage: www.elsevier.com/locate/ijhmt

Towards optimization of a pyroelectric energy converter for harvesting waste heat

Ashcon Navid, Damien Vanderpool, Abubakarr Bah, Laurent Pilon*

Mechanical and Aerospace Engineering Department, Henry Samueli School of Engineering and Applied Science, University of California, Los Angeles, CA 90095, USA

ARTICLE INFO

Article history:

Received 4 December 2009
 Received in revised form 6 April 2010
 Accepted 16 April 2010
 Available online 2 June 2010

Keywords:

Pyroelectric materials
 Direct energy conversion
 Waste heat harvesting
 Ferroelectric materials
 Oscillating flow

ABSTRACT

This paper reports numerical simulations of a prototypical pyroelectric energy converter as a novel approach for directly converting waste heat into electricity. The two-dimensional mass, momentum, and energy equations were solved to predict the local time-dependent pressure, velocity, and temperature. Then, heat input, pumping power, and electrical power generated were estimated, along with the thermodynamic energy efficiency and power density of the device. It was established that reducing the length of the device and/or the viscosity of the working fluid improved the energy efficiency and power density of the device by increasing the optimum operating frequency. Results show that a maximum efficiency of 5.2% at 0.5 Hz corresponding to 55.4% of the Carnot efficiency between 145 and 185 °C can be achieved with commercial 1.5 cst silicone oil as the working fluid and PZST as the pyroelectric material. The associated power density was found to be 38.4 W/L of material.

© 2010 Elsevier Ltd. All rights reserved.

1. Introduction

Industrial and developing nations are facing the challenges of meeting rapidly expanding needs for energy while minimizing impact to the environment. Power, refrigeration, and heat pump cycles release large amounts of waste heat as required by the second law of thermodynamics. For example, over 50% of the energy consumed by the United States in 2002 was lost in the form of waste heat typically at low temperatures [1]. Unfortunately, not many solutions exist for low grade waste heat harvesting due to the associated small Carnot efficiencies. Organic Rankine cycles use organic working fluids such as refrigerants and hydrocarbons instead of water to harvest waste heat at temperatures up to 200–300 °C [2]. Alternatively, Stirling engines can directly convert thermal energy into mechanical energy. They have been used in a variety of applications including heat pumps, cryogenic refrigeration, and air liquefaction [3]. In the last several decades, direct energy conversion technologies, such as thermoelectric devices have received significant attention [4]. They make use of the Seebeck effect to convert a steady-state temperature difference at the junction of two dissimilar metals or semiconductors into electrical energy [4]. Instead of using spatial temperature gradients, pyroelectric energy conversion directly converts time-dependent temperature oscillations into electricity [5–17]. It makes use of the pyroelectric effect to create a flow of charge to or from the surface of a material as a result of successive heating and cooling. Prototypical pyroelectric converters have been assembled and operated

in the past [5–10,18]. These devices consisted of a hot and a cold source separated by a series of microchannels supporting pyroelectric thin films and their electrodes. A working fluid oscillated between the hot and cold sources through the channels to create the required time-dependent temperature oscillations within the pyroelectric films. This paper reports numerical simulations of a device similar to that built by Olsen et al. [8] to investigate the effect of structural material properties, geometry, and fluid viscosity on the energy efficiency and power density of the device.

2. Current state of knowledge

2.1. Pyroelectric materials

Pyroelectric materials are materials that possess a so-called spontaneous polarization \mathbf{P}_s , defined as the electric dipole moment per unit volume averaged over the volume of the material, in the absence of an applied electric field. It depends strongly on temperature due to the material's crystallographic structure [19]. At steady-state ($dT/dt = 0$), the spontaneous polarization is constant. However, when the material is heated ($dT/dt > 0$), the spontaneous polarization decreases as dipole moments begin to lose their orientation. As a result, the charges stored at the surface of the material decreases resulting in the flow of current through an external circuit. When the material is cooled ($dT/dt < 0$), the dipole moments regain their orientation which increases the spontaneous polarization and allows for more charges to be stored at the surface of the material, thereby reversing the current flow. For some pyroelectric materials, the spontaneous polarization can be switched from \mathbf{P}_s to $-\mathbf{P}_s$ by reversing the applied coercive electric field. These materials

* Corresponding author. Tel.: +1 310 206 5598; fax: +1 310 206 4830.
 E-mail address: pilon@seas.ucla.edu (L. Pilon).

Nomenclature

$A_{1,2}$	surface area of pyroelectric elements PE ₁ and PE ₂ (m ²)	T_{Curie}	Curie temperature (°C)
A_c	cross-sectional area of fluid flow for one channel (m ²)	T_C	temperature of cold source (°C)
A_{hb}	area of heating band ($d \times L_H$) (m ²)	T_{cool}	cold temperature of pyroelectric element (°C)
A_p	cross-sectional area of piston (m ²)	T_H	temperature of hot source (°C)
c_p	specific heat (J/kgK)	T_{hot}	hot temperature of pyroelectric element (°C)
d	channel depth (m)	ΔT	temperature swing (°C)
D_h	hydraulic diameter ($= 4w_f$) (m)	u	velocity in the x-direction (m/s)
E	electric field (V/m)	v	velocity in the z-direction (m/s)
f	frequency (Hz)	V	voltage (V)
g	gravity (m/s ²)	V_L	low applied voltage (V)
k	thermal conductivity (W/mK)	V_H	high applied voltage (V)
L	total length of wall (m)	\forall	volume (m ³)
L_C	length of heat exchanger (m)	w	half-width (m)
L_H	length of heating band (m)	\dot{W}_E	generated electrical power (W)
L_{cr}	length of aluminum oxide plate (m)	\dot{W}_p	pumping power (W)
L_{PE}	length of pyroelectric element (m)	x	transverse coordinate in (x,z) coordinate system
N	number of internal walls supporting pyroelectric elements	z	vertical coordinate in (x,z) coordinate system
\overline{Nu}_f	space-cycled average Nusselt number	z_h	distance from transverse axis to heating band (m)
p	pressure (Pa)		
p_0	atmospheric pressure at free surface (Pa)	Greek symbols	
P_D	power density (W/L)	α	thermal diffusivity [$=k/(\rho c_p)$]
Pr	Prandtl number ($=\nu/\alpha$)	η	thermodynamic efficiency (%)
P_S	spontaneous polarization (C/m ²)	η_{Carnot}	Carnot efficiency (%)
PE	pyroelectric element	ν_f	kinematic viscosity (m ² /s)
q''_{in}	heat flux at heating band (W/m ²)	ρ	density (kg/m ³)
q	charge (C/m ²)	τ	period of oscillation ($=1/f$) (s)
Q_{in}	heat transfer rate into pyroelectric converter (W)		
Re_f	Reynolds number for oscillatory flow ($=2\pi fS^2/\nu_f$)	Subscripts	
S	piston stroke length (m)	A	refers to point A
S'	amplitude of working fluid in channel (m)	B	refers to point B
St	Strouhal number ($=D_h/S'$)	cr	refers to aluminum oxide plate
St_L	Strouhal number with respect to channel length ($=L/S'$)	f	refers to working fluid
t	time (s)	p	refers to piston
T	temperature (°C)	PE	refers to pyroelectric element
		w	refers to wall

are called ferroelectric materials. Note that all ferroelectric materials are pyroelectric but the converse is not true. Furthermore, the relationship between charge q and voltage V for a ferroelectric material exhibits hysteresis as shown in Fig. 1 for lead zirconate stannate titanate (PZST) of composition, $Pb_{0.99}Nb_{0.02}(Zr_{0.68}, Sn_{0.25}, Ti_{0.07})_{0.98}O_3$, between 152 and 194 °C. When the voltage is cycled across the material isothermally, the loops move in a counter-clockwise direction and the area enclosed by each loop represents the electrical energy dissipated. Beyond the Curie temperature, a ferroelectric material undergoes a phase transition from ferroelectric to paraelectric where the spontaneous polarization vanishes, resulting in the discharge of large electrical energy. In order to study the effect of structural material properties, geometry, and fluid viscosity on the performance of the device built by Olsen et al. [8] and to make quantitative comparisons to the original design, this study uses the same pyroelectric material namely PZST.

The converse of the pyroelectric effect is the electrocaloric effect. It is the change in temperature caused by a change in applied electric field under adiabatic conditions [19]. Sebald et al. [15] have shown that materials with large electrocaloric activity are of interest to pyroelectric energy harvesting. Large electrocaloric effects have recently been demonstrated. For example, a temperature change of 12 K in 350 nm thick zirconium rich $Pb(Zr,Ti)O_3$ (PZT) thin films was calculated for a change in electric field from 295 to 776 kV/cm near the Curie temperature of 220 °C [20]. Furthermore, Mischenko et al. [21] demonstrated large electrocaloric

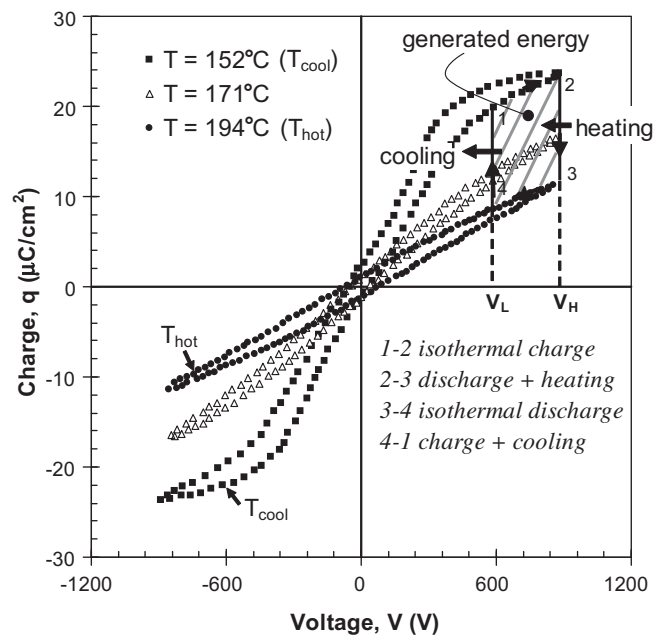


Fig. 1. Polarization versus applied voltage curves for PZST at different temperatures as reported in Ref. [35]. The Olsen cycle is represented by the shaded area enclosed by points 1–2–3–4.

activity near room temperature with 260 nm thick $0.9\text{PbMg}_{1/3}\text{Nb}_{2/3}\text{O}_3\text{-}0.1\text{PbTiO}_3$ (0.9PMN–0.1PT) thin films. The authors reported a 5 K temperature change as the electric field increased from 588 to 895 kV/cm near the Curie temperature of 60 °C. Similarly, studies on 210 nm thick 0.93PMN–0.07PT films suggest the possibility of a 9 K temperature change between 0 and 723 kV/cm near 25 °C [22]. In addition, 1 μm thick terpolymer poly(vinylidene fluoride-trifluoroethylene-chlorofluoroethylene) [P(VDF-TrFE-CFE)] films of composition 59.2/33.6/7.2 mol.% demonstrated a 9 K temperature change between 0 and 300 MV/m near 45 °C [23].

2.2. Pyroelectric energy conversion

Pyroelectric energy conversion using the Olsen cycle [5] is achieved by alternatively placing a pyroelectric material sandwiched between two electrodes in contact with a hot and cold source while applying the proper voltage V_L and V_H to perform the cycle shown in Fig. 1. The points 1–2–3–4 in the q - V diagram represent the electric analogue of the Ericsson cycle, with the area between 1–2 and 3–4 corresponding to the electrical energy produced by the material when the voltage is cycled between V_L and V_H and the temperature oscillates between T_{hot} and T_{cool} [9]. Stirling cycles are also possible [9,16], however, it has been shown experimentally that Ericsson cycles produce more power than Stirling cycles for PZST operating in the temperature and voltage range considered in this study [24]. The efficiency and power output of the Olsen cycle can be significantly improved by using multistaging and heat regeneration [8,9]. Multistaging consists of placing different pyroelectric elements (PEs) in series with increasing Curie temperature from the cold to hot sources. Heat regeneration is achieved by placing the PE in contact with a working fluid that oscillates between the hot and cold sources. As a result, the heat required to increase the temperature of the lattice is regenerated back and forth between the oscillating working fluid and the PE instead of being lost to the heat sink.

Furthermore, it was theoretically established that pyroelectric energy conversion using the Olsen cycle and heat regeneration can reach the Carnot efficiency between a hot and a cold thermal reservoir [8,25]. Limitations in reaching the Carnot efficiency include (i) hysteretic and resistive losses, (ii) heat losses to the surroundings, and (iii) sensible (thermal) energy [8,25].

In the early 1980's, Olsen and co-workers [5–7] built several prototypical pyroelectric converters and experimentally demonstrated 1 and 40 mW devices with efficiencies of approximately 0.4% but 16 times greater than the maximum efficiency predicted by van der Ziel [26]. Their devices operated between 145 and 178 °C, using PZST as the pyroelectric material and various silicone oils as the working fluid with viscosities between 50 and 200 cst. Ceramic stacks were used to create microchannels to ensure laminar flow of the fluid over the pyroelectric materials and to reduce axial heat conduction between the hot and cold sources. Later, Olsen et al. [8] constructed the only multistage device built to date using different grades of PZST that produced a maximum power density of 33 W/L of pyroelectric material at 0.26 Hz and achieved a maximum efficiency of 1.05% at 0.14 Hz, corresponding to 12% of the Carnot efficiency. Due to the cost of PZST (\sim \\$10,000/W), Olsen et al. [10] used poly(vinylidene fluoride-trifluoroethylene) [P(VDF-TrFE)] films 30–70 μm thick, rolled into a spiral stack and placed inside a cylindrical chamber containing silicone oil. The device was operated between 20 and 90 °C and produced an energy density of 30 J/L of P(VDF-TrFE) per cycle. In all these devices, the fluid was pumped by a step motor with a piston stroke length of 7.8–10 cm.

In addition, Olsen et al. [24] numerically simulated a pyroelectric converter by determining the heat transfer rate and temperature variations of the channel walls for peak-to-peak stroke

lengths of 2.8, 5.1, and 8.5 cm and frequencies between 0 and 0.6 Hz. Only the energy equation was solved assuming that (1) all of the channel walls were made of Al_2O_3 , (2) the flow was one-dimensional, laminar, fully developed, and oscillated with a parabolic velocity profile across the converter's channel, (3) axial heat conduction along the converter's walls was negligible, and (4) the heating and cooling heat exchangers were at constant temperatures and placed directly above and below the pyroelectric material. The authors determined that the numerically predicted heat transfer rate was in good agreement with experimental measurements at all frequencies for stroke lengths smaller than 2.8 cm. However, for larger stroke lengths, it became increasingly inaccurate (by up to 50%). This could be attributed to the simplifying assumptions previously listed. For example, the velocity profile of the working fluid was not fully developed along the microchannels but was in fact constant across the channel width at the piston/fluid interface. Moreover, axial heat conduction took place along the composite wall between the hot and cold sources. The experimental hot source operated at constant heat flux [8] instead of constant temperature as simulated numerically in Ref. [24]. Finally, the heating and cooling heat exchangers were not directly above and below the pyroelectric plates as simulated but were separated by 1.905 and 5.08 cm long walls of Al_2O_3 , respectively in the actual prototype [8].

More recently, Vanderpool et al. [27] completed two-dimensional numerical simulations of the prototypical pyroelectric converter experimentally assembled by Olsen et al. [8] in order to identify key design and operating parameters to increase the power output and the thermodynamic efficiency of the device. It was established that [27]:

1. the simulated efficiency fell within 29% of experimental data at all frequencies and optimum stroke length of 3.9 cm,
2. the mass, momentum, and energy equations must be solved simultaneously in order to compute the pumping power and accurately predict the temperature oscillations of the PE's,
3. the pyroelectric converter operated less efficiently at frequencies greater than 0.1 Hz because the heat input increased more rapidly than the generated electrical power,
4. the efficiency of the pyroelectric converter increased with smaller values of the heat capacity of the working fluid and of the PE. It was established that a maximum efficiency of 3.4% corresponding to 40.3% of the Carnot efficiency could be achieved at 0.062 Hz by dividing the heat capacity of both the PE and the working fluid by a factor of 2, and
5. the power density of the pyroelectric converter increased with larger frequencies, smaller values of the heat capacity of the PE, and larger values of the heat capacity of the working fluid.

The heat capacity of the pyroelectric material can be reduced by making the material porous [28]. However, porosity can reduce the dielectric strength of the material, limiting the high voltage V_H used in the Olsen cycle. Furthermore, it is difficult to reduce the heat capacity of the working fluid as it does not vary significantly from one fluid to another [29]. Thus, it is of practical significance to identify other design parameters which can improve the performance of the device and can be more easily implemented experimentally. Therefore, this paper expands the study of Vanderpool et al. [27] by investigating the effect of structural material properties, geometry, and fluid viscosity on the efficiency and power density of the device experimentally built by Olsen et al. [8]. First, to minimize heat losses and axial heat conduction between the hot and cold sources, the Al_2O_3 plates were replaced with anisotropic material, acting as a perfect thermal insulator in the fluid flow direction. Next, to raise the power density of the device, the optimum operating frequency was increased by reducing the length

of the Al_2O_3 plates that make up the channel walls to obtain an overall length that was half as long as that of the original device [8]. Finally, to reduce the pumping power which can become significant at higher operating frequencies, the 50 cst silicone oil working fluid was replaced with commercially available 1.5 cst silicone oil of much lower viscosity [29].

3. Analysis

3.1. Direct pyroelectric conversion system

The prototypical pyroelectric converter based on the Olsen cycle [8] consisted of thermal and electrical sub-systems. The thermal sub-system was used to create a time-dependent temperature oscillation which heated the PEs to a maximum temperature T_{hot} and cooled them to a minimum temperature T_{cool} . The electrical sub-system controlled the electric field applied to the PEs to per-

form the Olsen cycle. It also collected the charges generating by cooling and heating the PEs.

3.1.1. Thermal sub-system

Fig. 2 shows a cross-section of the simulated prototypical pyroelectric converter [8] of length L along with the dimensions and coordinate system. The device consisted of N equally spaced internal walls placed inside the device to form $(N + 1)$ micro-channels. The walls were made from four plates stacked vertically. The top and bottom plates were identical and made of Al_2O_3 while the middle plates were made of pyroelectric material PZST. The channels were filled with the working fluid and a piston-in-a-cylinder pump was used to oscillate the working fluid vertically between a cold source and a hot source. Moreover, the pump featured adjustable stroke length S and operating frequency f . At the bottom of the channels, the cold source was a heat exchanger maintained at temperature T_C . The hot source

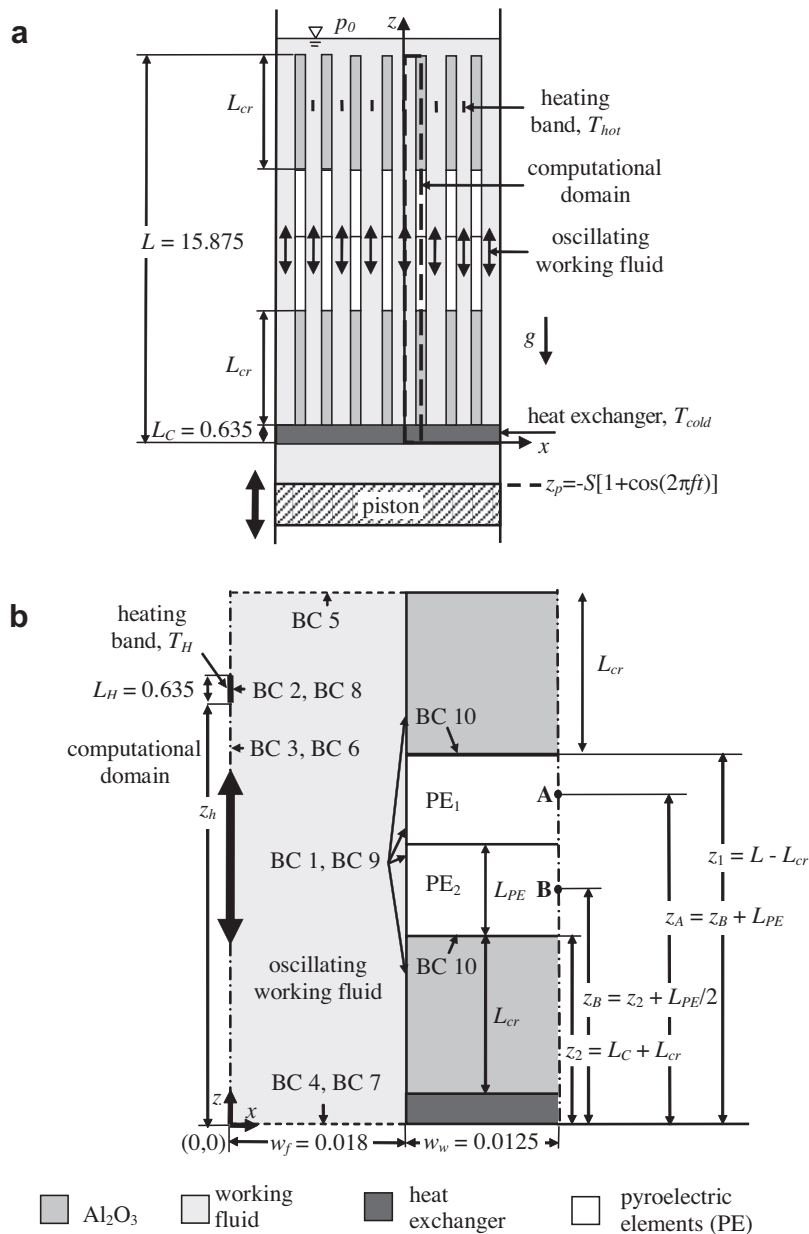


Fig. 2. (a) Schematic of the overall pyroelectric converter of length L , (b) schematic of the computational domain along with the coordinate system and the boundary conditions (all dimensions in cm).

was a thin heating band at temperature T_H , numerically simulated as a line source, operating at constant heat flux q''_h . It was used to heat the working fluid at the top of the channels. Each channel had a total length L and half-widths for the channel and wall denoted by w_f and w_w , respectively and a depth $d = 3.8$ cm [8]. In addition, the length of the top and bottom Al_2O_3 wall plates was denoted by L_{cr} . The heat exchanger had length L_C while the heating band, located at height z_h , had length L_H . The vertical locations of the PZST plates PE_1 and PE_2 were denoted by $z_1 = (L - L_{cr})$ and $z_2 = (L_C + L_{cr})$, respectively, while the centers of the PEs were marked by points A and B at a height of z_A and z_B , respectively. The location of the top surface of the piston was given by $z_p = -S[1 + \cos(2\pi ft)]$. The stroke length S was chosen such that when the piston was at its maximum height of $z_p = 0$, a fluid particle at the top of the heating band $z = (z_h + L_H)$ would travel down to $z = z_2$ when the piston was at its lowest point $z_p = -2S$. Larger stroke lengths would create heat losses while smaller ones would reduce the temperature swing experienced by the PEs.

3.1.2. Electrical sub-system

The electrical sub-system used for the PEs was the same as that used by Olsen et al. [9]. Briefly, both faces of each PE were plated with electrodes and connected to an electrical circuit which measured the charge and the applied electric field of the PE. The circuit consisted of a Sawyer–Tower bridge [30] which measured the charge of the pyroelectric material and a resistive voltage divider placed in parallel to the Sawyer–Tower bridge to monitor the electric field applied to the material. Voltages V_L and V_H were applied to the PEs and synchronized with the temperature to maintain the desired low or high electric fields E_L and E_H required to perform the Olsen cycle (Fig. 1).

3.2. Assumptions

The same assumptions made by Vanderpool et al. [27] were also made here to make the problem mathematically trackable:

1. The entire device was well insulated so heat losses to the surrounding and between channels were negligible.
2. All material properties for the wall and the working fluid were assumed to be constant.
3. The working fluid, namely silicone oil, was treated as an incompressible Newtonian fluid.
4. The spacing between the walls was much smaller than the depth of the plates so that two-dimensional flow prevailed.
5. The Reynolds number of the periodically oscillating fluid flow for all simulations was much less than the critical Reynolds number for oscillating flow so that the fluid flow was laminar [31].
6. Edge effects were neglected. In other words, all channels were equivalent and only one was simulated.
7. As a first order approximation, the thin metallic electrodes deposited on the PE plates to collect the generated current were assumed to have no effect on the heat transfer and fluid flows.
8. Due to the lack of thermophysical properties for various doping levels of PZST, the PEs at the two stages of the converter were assumed to be identical.

3.3. Governing equations

The two-dimensional mass and momentum conservation equations for an incompressible Newtonian fluid with constant properties in Cartesian coordinates were solved to determine the velocity components and pressure field of the working fluid. They are expressed as [32],

$$\frac{\partial u_f}{\partial x} + \frac{\partial v_f}{\partial z} = 0 \quad (1)$$

$$\frac{\partial u_f}{\partial t} + u_f \frac{\partial u_f}{\partial x} + v_f \frac{\partial u_f}{\partial z} = -\frac{1}{\rho_f} \frac{\partial p_f}{\partial x} + \nu_f \left(\frac{\partial^2 u_f}{\partial x^2} + \frac{\partial^2 u_f}{\partial z^2} \right) \quad (2)$$

$$\frac{\partial v_f}{\partial t} + u_f \frac{\partial v_f}{\partial x} + v_f \frac{\partial v_f}{\partial z} = -\frac{1}{\rho_f} \frac{\partial p_f}{\partial z} + \nu_f \left(\frac{\partial^2 v_f}{\partial x^2} + \frac{\partial^2 v_f}{\partial z^2} \right) - g \quad (3)$$

where ρ_f and ν_f are the density and kinematic viscosity of the working fluid, respectively. The x - and z -components of the velocity vector are denoted by u_f and v_f , respectively, while p_f is the local fluid pressure, and g is the gravitational acceleration ($=9.81$ m/s²).

The temperature $T_f(x, z, t)$ within the working fluid at location (x, z) and time t was determined by solving the two-dimensional energy equation written as [32],

$$\rho_f c_{p,f} \left(\frac{\partial T_f}{\partial t} + u_f \frac{\partial T_f}{\partial x} + v_f \frac{\partial T_f}{\partial z} \right) = k_f \left(\frac{\partial^2 T_f}{\partial x^2} + \frac{\partial^2 T_f}{\partial z^2} \right) \quad (4)$$

where $c_{p,f}$ and k_f are the fluid heat capacity and thermal conductivity, respectively. These properties were assumed to be constant.

Finally, the two-dimensional heat diffusion equation for the wall material and the PZST plates that made up the channel walls was expressed as,

$$\rho_w c_{p,w} \frac{\partial T_w}{\partial t} = k_{w,x} \frac{\partial^2 T_w}{\partial x^2} + k_{w,z} \frac{\partial^2 T_w}{\partial z^2} \quad (5)$$

where the subscript w refers to either the walls or the PEs. The thermal conductivities were assumed to be independent of temperature but could be anisotropic as suggested by the subscripts in $k_{w,x}$ and $k_{w,z}$.

3.4. Initial and boundary conditions

Initially ($t = 0$), the working fluid was at rest. Thus, for $0 \leq x \leq w_f$ and $0 \leq z \leq L$,

$$u_f(x, z, 0) = v_f(x, z, 0) = 0 \quad (6)$$

In addition, at $t = 0$, the temperature of the working fluid was assumed to vary linearly between the heating band at $z = z_h$ and temperature T_H and the heat exchanger at $z = L_C$ and temperature T_C and did not vary in the x -direction. Furthermore, along the heating band and exchanger, the temperature profile of the working fluid was constant. Thus, for $0 \leq x \leq w_f + w_w$,

$$T_f(x, z, 0) = T_w = \begin{cases} T_C & \text{for } 0 \leq z \leq L_C \\ T_C + \frac{(T_H - T_C)(z - L_C)}{z_h - L_C} & \text{for } L_C \leq z \leq z_h \\ T_H & \text{for } z_h \leq z \leq L \end{cases} \quad (7)$$

The mass, momentum, and energy equations were subject to the boundary conditions (BC) listed in Tables 1 and 2. Note that for the fluid–piston interface (BC 5 in Table 1) and for $z < 0$, the velocity of the working fluid was equal to the velocity of the piston, given by $v_p = 2\pi f S \sin(2\pi ft)$. From mass conservation considerations and assuming that the fluid was incompressible, the velocity of the fluid at the bottom inlet of the channels was uniform and a sinusoidal function of time with amplitude $S' = (SA_p)/[(N + 1)A_c]$, where A_p and A_c were the cross-sectional area of the piston and of a single channel, respectively.

3.5. Properties

The thermophysical properties of Al_2O_3 , PZST, and of the two working fluids investigated in this study, namely commercial 50 and 1.5 cst silicone oil by Dow Corning [29], were assumed to be constant over the temperature range simulated. Note that the relative differences in the material properties were less than 10% be-

Table 1
Boundary conditions associated with the two-dimensional mass and momentum equations [Eqs. (1)–(3)].

Boundary	Boundary condition	No.
Walls	$u_f(w_f, z, t) = 0,$ $v_f(w_f, z, t) = 0,$ for $0 \leq z \leq L$	BC 1
Heating band	$u_f(0, z, t) = 0, v_f(0, z, t) = 0,$ for $z_h \leq z \leq (z_h + L_H)$	BC 2
Channel center line	$u_f(0, z, t) = \frac{\partial v_f}{\partial x}(0, z, t) = 0,$ for $0 \leq z \leq z_h, (z_h + L_H) \leq z \leq L$	BC 3
Fluid-piston interface	$u_f(x, 0, t) = 0,$ $v_f(x, 0, t) = 2\pi f S \sin(2\pi f t),$ for $0 \leq x \leq w_f$	BC 4
Fluid-air interface	$p_f(x, L, t) - p_0 = \rho g S [1 - \cos(2\pi f t)],$ for $0 \leq x \leq w_f$	BC 5

Table 2
Boundary conditions associated with the two-dimensional energy equation [Eq. (4)].

Boundary	Boundary condition	No.
Walls	$\frac{\partial T_f}{\partial x}(0, z, t) = \frac{\partial T_f}{\partial x}(w_f + w_w, z, t) = 0,$ for $0 \leq z \leq L$	BC 6
Heat exchanger	$T_c = T_f(x, 0, t),$ for $0 \leq x \leq w_f$	BC 7
Heating band	$q''(0, z, t) = q''_{in},$ for $z_h \leq z \leq (z_h + L_H)$	BC 8
Fluid-wall interface	$-k_f \frac{\partial T_f}{\partial x}(w_f, z, t) = -k_w \frac{\partial T_w}{\partial x}(w_f, z, t),$ for $0 \leq z \leq L$	BC 9
Al ₂ O ₃ -PE interface	$-k_{cr} \frac{\partial T_{cr}}{\partial x}(x, z_1 \text{ or } z_2, t) = -k_{pe} \frac{\partial T_{pe}}{\partial x}(x, z_1 \text{ or } z_2, t),$ for $w_f \leq x \leq w_f + w_w$	BC 10

tween $T_c=145^\circ\text{C}$ and $T_H=185^\circ\text{C}$ except for the kinematic viscosity of the 50 and 1.5 cst silicone oils which varied by up to 37% and 25%, respectively [29]. As a first order approximation, ν_f was evaluated at the arithmetic mean temperature of 165°C and assumed to be constant and equal to 8.29 and $0.48\text{ mm}^2/\text{s}$ [29] for the 50 and 1.5 cst silicone oil, respectively. Similarly, the density, specific heat, and thermal conductivity of Al₂O₃, 50 and 1.5 cst silicone oils were also estimated at 165°C and obtained from Refs. [33] and [29]. Unfortunately, for PZST, the density, specific heat, and thermal conductivity were only available in literature at room temperature [34]. However, its q - V curve was linearly interpolated from data taken from Ref. [35] at the temperature computed in the pyroelectric elements PE₁ and PE₂. The material properties of Al₂O₃, PZST, 50 and 1.5 cst silicone oils used in this study are summarized in Table 3.

3.6. Method of solution

The method of solution and validation of the numerical tools were reported elsewhere [27] and need not be repeated. In brief, the transient mass, momentum, and energy conservation equations were solved simultaneously using the finite element solver COMSOL 3.5a applying the Galerkin finite element method on

Table 3
Fluid and material properties used in the numerical simulations [29,33,34].

Property	Silicone oil (50 cst) [29] at 165°C	Silicone oil (1.5 cst) [29] at 165°C	PZST [34] at 25°C	Al ₂ O ₃ [33] at 165°C
ρ (kg/m ³)	761.6	716.6	7750	3970
c_p (J/kgK)	1913.3	1931.2	350	972.4
k (W/mK)	0.157	0.109	1.1	24.4
ν_f (mm ² /s)	8.29	0.48	-	-

structured rectangular meshes. A Dell Precision 690 computer with eight 2.66 GHz processors, and 40 GB of RAM was used to run the simulations.

3.7. Performance analysis

The total electrical power generated by the two PEs in all channels was determined as,

$$\dot{W}_E = Nf \left(\oint V_1 A_1 dq_1 + \oint V_2 A_2 dq_2 \right) \quad (8)$$

where N was the total number of internal walls and f was the frequency (in Hz). The surface areas A_1 and A_2 of each pyroelectric plate were both equal to 9.652 cm^2 . The shaded area in Fig. 1 graphically illustrates the integral $\oint V dq$. To determine the charge-voltage curve at the temperatures T_{cool} and T_{hot} computed at points A and B (Fig. 2), linear interpolation of the charge-voltage curves at temperatures 152, 171, and 194°C shown in Fig. 1 for PZST [35] was used. Due to a lack of experimental data for the charge-voltage curves, PE₁ and PE₂ were assumed to be made of the same material and, therefore, had the same charge-voltage curves. The device operated between voltages V_L and V_H equal to 100 and 700 V, respectively [8].

The pumping power required to pump the working fluid through the channels was assumed to be only due to frictional losses within the channel. Therefore, the total pumping power time averaged over the period $\tau(=1/f)$ was defined as,

$$\dot{W}_p \approx \frac{(N+1)}{\tau} \int_0^\tau \left(\int_{A_c} p_f v_f dA \right) dt \quad (9)$$

where the local instantaneous fluid velocity v_f and pressure p_f were determined by solving the mass and momentum conservation equations. Integration in Eqs. (8) and (9) was performed numerically using the trapezoidal rule.

Moreover, the total heat transfer rate provided by the heating band was computed as,

$$\dot{Q}_{in} = 2(N+1)q''_{in}A_{hb} \quad (10)$$

where A_{hb} is the surface area of the heating band in one channel and equal to 2.413 cm^2 .

Furthermore, the average thermodynamic energy efficiency of the system over one cycle was defined as,

$$\eta = \frac{\dot{W}_{cycle}}{\dot{Q}_{in}} = \frac{\dot{W}_E - \dot{W}_p}{\dot{Q}_{in}} \quad (11)$$

Note that all other losses such as heat losses to the surrounding and current leakages in the electrical circuit were neglected for the sake of simplicity.

Finally, the power density of the device, representing the total amount of electrical power generated per unit volume of PEs, was determined as

$$P_D = \frac{\dot{W}_E}{2N\nabla_{PE}} \quad (12)$$

Each internal wall supported two PEs of volume ∇_{PE} so the total volume of PEs in the device was $2N\nabla_{PE}$. In this study, the number of internal walls was $N = 100$ as achieved experimentally [8].

4. Results and discussion

In order to optimize the performance of the device, the following four cases were considered:

1. Case 1 was the same baseline case as that discussed by Vanderpool et al. [27].

2. Case 2 explored the use of spacer material with anisotropic thermal conductivity to minimize heat losses by reducing axial heat conduction through the microchannel walls separating the hot and cold sources. To do so, Al_2O_3 was replaced by spacer plates with anisotropic thermal conductivity such that $k_{w,x} = k_{\text{Al}_2\text{O}_3}$ and $k_{w,z} = 0 \text{ W/mK}$. All other parameters were the same as Case 1.
3. Case 3 aimed to increase the power density by raising the optimum operating frequency. To do so, the length of the device was reduced from L to $L/2$ by reducing the length of the Al_2O_3 wall plates L_{cr} from 5.08 to 1.00 cm. The stroke length S was reduced from 3.9 to 3.04 cm in order to maintain the optimum stroke length discussed in Section 3.1.1. All other parameters were the same as Case 1.
4. Case 4 examined the use of a less viscous working fluid to reduce the pumping power which can become significant at higher frequencies. To do so 50 cst silicone oil was replaced with commercially available 1.5 cst silicone oil as the working fluid which had similar ρc_p values but a viscosity 33 times less than that of 50 cst silicone oil [29]. All other parameters were the same as Case 3.

In all cases, the heat flux q''_{in} was adjusted by trial and error to maintain the heater band at temperature $T_H = 185 \pm 7 \text{ }^\circ\text{C}$.

4.1. Heat transfer rate and temperature oscillations

Fig. 3 plots the heat transfer rate \dot{Q}_{in} required to maintain the heater temperature at $185 \pm 7 \text{ }^\circ\text{C}$ as a function of piston frequency for Cases 1 through 4. Note that the lines in all figures are intended only to guide the eyes. Frequencies above 0.2 Hz were not simulated for Cases 1 and 2 since the efficiency became vanishingly small as discussed later. Similarly for Cases 3 and 4, frequencies larger than 0.85 Hz were not explored.

For Cases 1 and 2, \dot{Q}_{in} increased rapidly as a function of frequency and, in fact, was the same in both cases. Thus, replacing Al_2O_3 with an anisotropic material did not affect \dot{Q}_{in} . Indeed, the PZST plates, forming the midsection of the microchannel walls, had a thermal conductivity of 1.1 W/mK which provided good

thermal insulation between the hot and cold sources in both cases. The different trends in \dot{Q}_{in} versus frequency observed for Cases 3 and 4 can be explained by examining how stroke length affects heat transfer in the device. Ozawa et al. [36] numerically and experimentally explored forced convection in laminar oscillating fluid flows under uniform heat flux. Through numerical simulations, the effects of Reynolds number Re_f , Prandtl number Pr_f , stroke length S' , and channel length L were explored. The authors reported the following correlation for the surface- and time-average Nusselt number $\overline{\text{Nu}}_f$ [36],

$$\overline{\text{Nu}}_f = 0.92\text{St}^{-0.2}\text{St}_L^{-0.26}\text{Pr}_f^{0.4}\text{Re}_f^{0.44} \quad \text{for } \text{Re}_f < 2450/\text{St} \quad (13)$$

where $\text{St} = D_h/S'$ is the Strouhal number, D_h is the hydraulic diameter, $\text{St}_L = L/S'$ is the Strouhal number with respect to channel length, $\text{Pr}_f = \nu_f/\alpha_f$ is the Prandtl number where $\alpha_f = k_f/\rho_f c_{p,f}$ is the thermal diffusivity of the working fluid, and $\text{Re}_f = 2\pi f S'^2/\nu_f$ is the Reynolds number in oscillatory flow. The correlation was in good agreement with experimental data obtained using water and for pipes of various diameters [36]. For Case 3 of the present study, the heat transfer coefficient $h = \overline{\text{Nu}}_f k_f/D_h$ was 14% less than that for Cases 1 and 2 at a given frequency. This was due to the fact that the stroke length was 22% less for the shorter device considered in Case 3. Indeed, reducing the stroke length reduced the Reynolds number Re_f by 39% at a given frequency and increased St by 28% compared to Cases 1 and 2. Thus, in shorter devices operating at low frequencies, heat transfer from the heater to the fluid is dominated by conduction over forced convection. Therefore, the heat transfer coefficient was smaller in Case 3 than in Cases 1 and 2 and \dot{Q}_{in} was not a strong function of frequency up to 0.5 Hz as illustrated in Fig. 3.

Moreover, using 1.5 cst silicone oil (Case 4) as the working fluid further decreased \dot{Q}_{in} by 50–62% compared to Case 3 for all frequencies. In fact, $\overline{\text{Nu}}_f$ computed from Eq. (13) was 27% greater for Case 4 than for Case 3 at a given frequency. However, the corresponding heat transfer coefficient h was 12% smaller. This was due to the fact that the thermal conductivity of 1.5 cst silicone oil was 30% less than that of 50 cst silicone oil. The reduction in heat transfer coefficient reduces the heat input \dot{Q}_{in} required to keep the heating band at $185 \text{ }^\circ\text{C}$. Furthermore, the reduction in fluid thermal conductivity helps minimize heat losses due to axial conduction within the working fluid which further decreases \dot{Q}_{in} . In addition, the heat capacity ρc_p for 1.5 cst silicone oil is 5% less than that for 50 cst silicone oil which results an additional reduction in \dot{Q}_{in} . While the difference in ρc_p is small, it can have a significant impact on the heat input \dot{Q}_{in} as reported by Vanderpool et al. [27]. For example, the authors found that reducing ρc_p by 50% lowered \dot{Q}_{in} by up to 76% [27].

Fig. 4 shows the temperature swing ΔT in the PEs at points A and B as a function of frequency. For all cases, ΔT_A and ΔT_B decreased as a function of frequency. This can be attributed to the thermal inertia of both the fluid and the PEs as well as reduction in thermal contact time between the heating band or heat exchanger and the working fluid and between the fluid and the PEs. Here also, Cases 1 and 2 showed similar values of ΔT_A and ΔT_B for all frequencies, indicating that replacing Al_2O_3 with an anisotropic material (Case 2) did not significantly affect either ΔT or \dot{Q}_{in} . On the contrary, reducing the length of the device (Case 3) increased ΔT_A and ΔT_B by at least 62% and 23%, respectively when compared to Case 1. This significant increase was due to larger \dot{Q}_{in} required to maintain the heating band at $185 \text{ }^\circ\text{C}$ (see Fig. 3). In addition, replacing the working fluid with 1.5 cst silicone oil (Case 4) decreased ΔT_A and ΔT_B by up to 36% and 30%, respectively, when compared to those of Case 3. This can be attributed to smaller values of \dot{Q}_{in} in Case 4 compared with Case 3 as shown in Fig. 3. Although \dot{Q}_{in} decreased between 50% and 62% from Case 3 to Case 4, ΔT_A and ΔT_B were reduced by less than 36% thanks to the reduction of axial conduction achieved using 1.5 cst silicone oil.

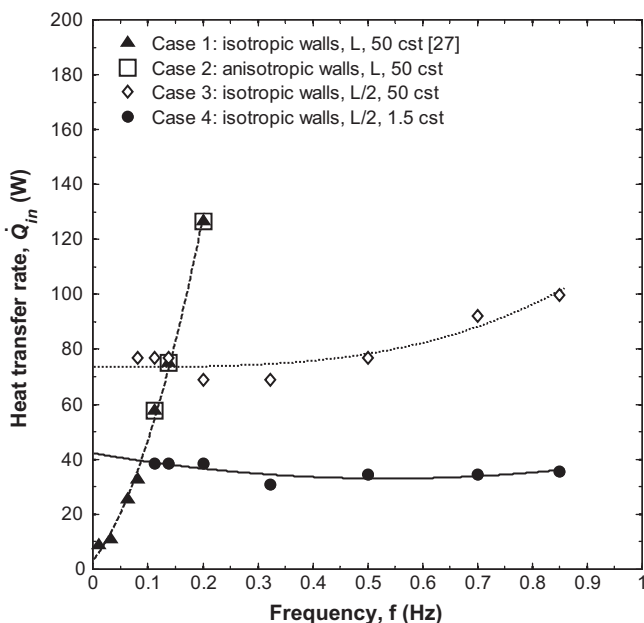


Fig. 3. Heat transfer rate \dot{Q}_{in} as a function of frequency f for Cases 1 through 4 required to maintain $T_H = 185 \pm 7 \text{ }^\circ\text{C}$.

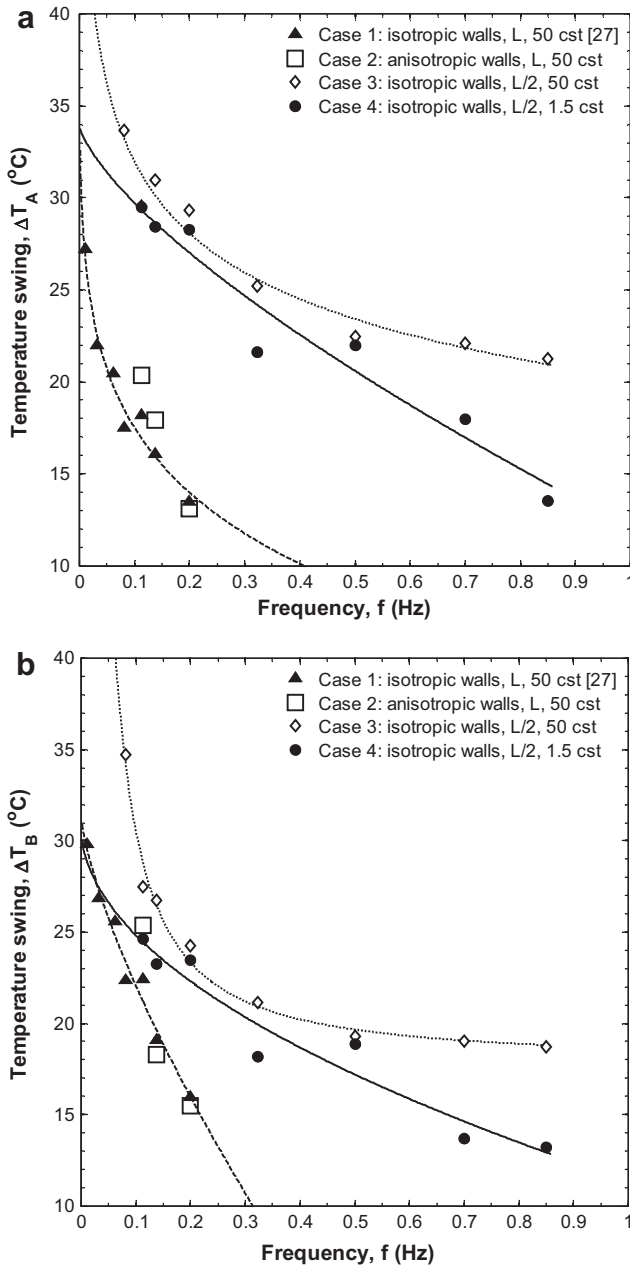


Fig. 4. Temperature swing at (a) point A and (b) point B as a function of frequency f for Cases 1 through 4 for $T_H = 185 \pm 7$ °C.

4.2. Generated electrical power and pumping power

Fig. 5a plots the generated electrical power \dot{W}_E estimated from Eq. (8) as a function of frequency for all cases. For Cases 1 and 2, \dot{W}_E increased with frequency and the generated electrical power was similar in both cases. Here also, replacing Al_2O_3 (Case 1) with an anisotropic material (Case 2) did not affect \dot{W}_E since Cases 1 and 2 featured similar values of \dot{Q}_{in} and ΔT . Decreasing the length of the device (Case 3), however, increased \dot{W}_E by at least 122% when compared to that of Cases 1 and 2 for a given frequency. The improvement was due to the larger temperature swings experienced by the PEs in Case 3. At 0.85 Hz, the generated electrical power reached 2.8 W, however, the efficiency was negative, as discussed in the following section. On the other hand, replacing the working fluid with 1.5 cst silicone oil (Case 4) decreased \dot{W}_E when compared to Case 3 for frequencies above 0.2 Hz as the tempera-

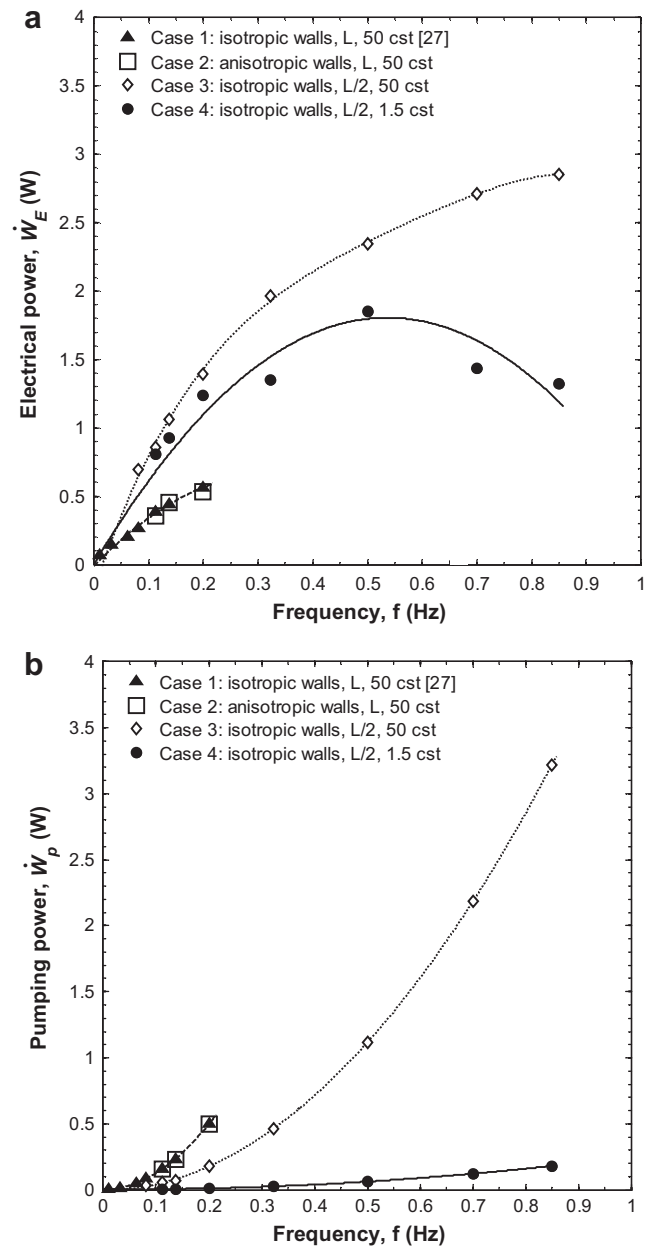


Fig. 5. (a) Generated electrical power \dot{W}_E , defined in Eq. (8), and (b) pumping power \dot{W}_p , defined in Eq. (9), as a function of frequency f for Cases 1 through 4.

ture swings ΔT_A and ΔT_B obtained in Case 4 were smaller than those in Case 3. A maximum \dot{W}_E of 1.9 W was achieved at 0.5 Hz in Case 4. For higher frequencies, \dot{W}_E decreased as the temperature swing rapidly decreased with frequency (see Fig. 4). Furthermore, the increase in optimum operating frequency for Cases 3 and 4 resulted in larger \dot{W}_E compared to Cases 1 and 2.

Fig. 5b shows the pumping power \dot{W}_p computed from Eq. (9) as a function of frequency for Cases 1 through 4. For all cases, \dot{W}_p was proportional to f^2 . Indeed, the velocity and pressure of the working fluid were proportional to f and f^2 , respectively [27,37]. Therefore, averaged over one cycle [Eq. (9)], the pumping power was found to be proportional to f^2 . For Cases 1 and 2, the pumping power was identical since both cases used the same working fluid with constant properties. For shorter device (Case 3), \dot{W}_p was between 64% and 71% smaller than that of Case 1 for a given frequency. This was due to the reduction in the channel length which resulted in smaller pressure drop. The latter was further reduced by

decreasing the fluid viscosity (Case 4). Thus, \dot{W}_p decreased by 91–95% as viscosity decreased from 50 cst (Case 3) to 1.5 cst (Case 4). Note that for 50 cst fluid viscosity (Cases 1–3), \dot{W}_p became comparable to \dot{W}_E at higher frequencies. In fact, \dot{W}_p was greater than \dot{W}_E beyond 0.85 Hz for Case 3. However, for fluid viscosity of 1.5 cst (Case 4), \dot{W}_p was negligible compared to \dot{W}_E for all frequencies investigated as illustrated in Fig. 5.

4.3. Efficiency and power density

For the simulated device operating between $T_C = 145^\circ\text{C}$ and $T_H \approx 185^\circ\text{C}$, the Carnot efficiency defined by $\eta_{\text{Carnot}} = 1 - T_C/T_H$ was approximately 8.7%. Fig. 6 shows the efficiency η and the efficiency ratio $\eta/\eta_{\text{Carnot}}$ as a function of frequency for each case considered. All cases exhibited similar behavior with η and $\eta/\eta_{\text{Carnot}}$

increasing with frequency, reaching a maximum, and then decreasing with further increase in frequency. At low frequencies, η and $\eta/\eta_{\text{Carnot}}$ increased with frequency since (a) \dot{W}_E increased at a faster rate than \dot{Q}_{in} and (b) \dot{W}_p was negligible compared with \dot{W}_E . However, at higher frequencies, η and $\eta/\eta_{\text{Carnot}}$ decreased since (i) \dot{Q}_{in} increased at a faster rate than \dot{W}_E and (ii) \dot{W}_p was no longer negligible compared with \dot{W}_E . Fig. 6 indicates that using anisotropic wall material (Case 2) did not improve η and $\eta/\eta_{\text{Carnot}}$ as observed for \dot{Q}_{in} , ΔT , \dot{W}_E , and \dot{W}_p . However, reducing the length of the device by half (Case 3) increased the maximum efficiency to 2.2% corresponding to an optimum operating frequency of 0.323 Hz and representing 25.9% of the Carnot efficiency. This was about 2 times greater than the maximum efficiency of 1.2% obtained at 0.031 Hz for Case 1 which corresponded to only 14.5% of the Carnot efficiency. The greater values of η and $\eta/\eta_{\text{Carnot}}$ for Case 3 were mainly due to the larger temperature swings which increased the electrical power generated by the pyroelectric materials. Note that beyond 0.85 Hz, η and $\eta/\eta_{\text{Carnot}}$ were negative as the pumping power became larger than the electrical power generated.

Moreover, reducing the viscosity of the fluid from 50 cst (Case 3) to 1.5 cst (Case 4) increased the maximum efficiency to 5.2% at 0.5 Hz corresponding to 55.4% of the Carnot efficiency. This was approximately a factor 2 greater than the maximum efficiency of Case 3. This further increase in efficiency was due to a significant reduction in (i) pumping power \dot{W}_p , observed in Case 4, which allowed the device to operate at higher frequencies and in (ii) heat input \dot{Q}_{in} needed to maintain the heating band at $T_H = 185^\circ\text{C}$ as previously discussed.

Fig. 7 plots the power density P_D as a function of frequency for Cases 1 through 4. For all cases, P_D was linearly proportional to frequency for small frequencies as suggested by Eqs. (8) and (12). Above 0.2 Hz, P_D was not linear with respect to frequency for Cases 3 and 4 as the temperature swing began to rapidly decrease (see Fig. 4). In fact, P_D began decreasing for Case 4 beyond 0.5 Hz. The figure indicates that using anisotropic material for the channel walls (Case 2) did not improve the power density as already observed with \dot{W}_E . However, reducing the length of the device (Cases 3 and 4) significantly increased P_D . This was due in part to the ability of the shortened device to achieve larger temperature swings in

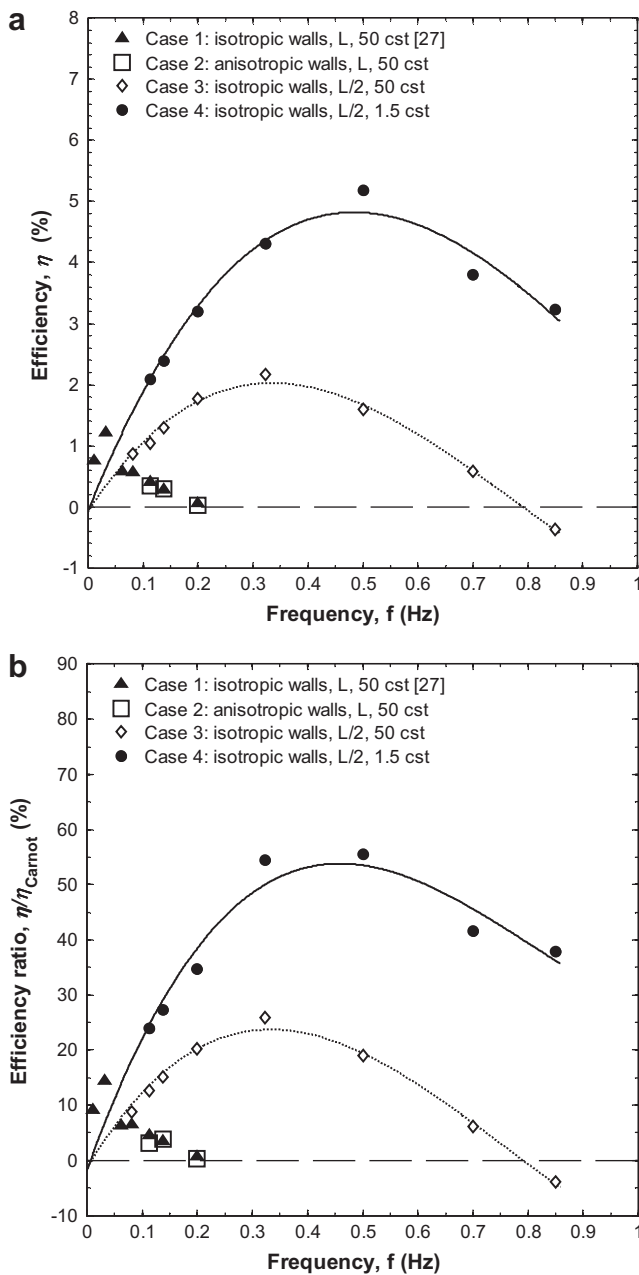


Fig. 6. (a) Efficiency η , defined in Eq. (11), and (b) efficiency ratio $\eta/\eta_{\text{Carnot}}$ as a function of frequency f for Cases 1 through 4. $\eta_{\text{Carnot}} = 8.73\%$ for $T_C = 145^\circ\text{C}$ and $T_H \approx 185^\circ\text{C}$.

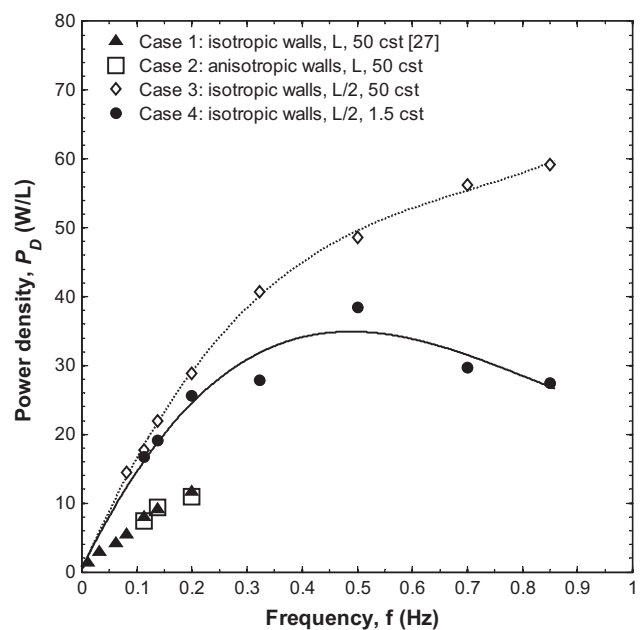


Fig. 7. Power density P_D , defined in Eq. (12), as a function of frequency f for Cases 1 through 4.

the PEs than Cases 1 and 2 for a given frequency. In addition, acceptable ΔT_A and ΔT_B were achieved at higher frequencies (see Fig. 4). Note that P_D obtained for Case 4 was less than that of Case 3 for all frequencies since the temperature swings and hence \dot{W}_E were smaller (see Fig. 5a). For Case 3, a power density of 59.2 W/L of pyroelectric material was achieved at 0.85 Hz but the efficiency was negative (see Fig. 6a). However, for lower fluid viscosity (Case 4) P_D reached a maximum of 38.4 W/L at 0.5 Hz.

Finally, it is of interest to compare the performance of the prototypical pyroelectric converter investigated with similar alternative technologies such as thermoelectric generators. Recently, Niu et al. [38] experimentally constructed a low temperature waste heat thermoelectric generator using commercially available Bi_2Te_3 thermoelectric modules and a parallel-plate heat exchanger. The authors achieved a maximum power density of 389 W/L of thermoelectric material and operated with an efficiency of 4.4% corresponding to 15.7% of the Carnot efficiency between 30 and 150 °C [38]. While their power density was 10 times greater than that obtained in Case 4, the efficiency ratio with respect to Carnot was lower. The large power density of the thermoelectric generator can be accredited to the much larger temperature differential and the correspondingly larger Carnot efficiency. The comparison suggests that pyroelectric energy conversion is a promising technology that should be further explored both experimentally and numerically. Focus should be given to developing materials with better performance, such as the recent efforts made by Refs. [20–23], and to systematically optimizing not only the length of the device but also all other design and operating parameters including the channel width and materials as well as frequency.

5. Conclusion

This study aimed at numerically assessing the effects of design parameters and operating conditions in order to improve the performance of pyroelectric energy converters based on the Olsen cycle. It was established that:

1. Eliminating axial heat conduction by replacing the aluminum oxide plates with a material featuring anisotropic thermal conductivity (Case 2) did not improve the performance of the device.
2. Shortening the device (Case 3) significantly improved its performance and allowed it to operate more efficiently at higher frequencies. A maximum efficiency of 2.2% at 0.323 Hz corresponding to 25.9% of the Carnot efficiency for a power density of 40.7 W/L of pyroelectric material was obtained using 50 cst silicone oil as the working fluid.
3. Not only shortening the device but also reducing the viscosity of the working fluid (Case 4) further improved the efficiency of the device. A maximum efficiency of 5.2% at 0.5 Hz corresponding to 55.4% of the Carnot efficiency and a power density of 38.4 W/L of pyroelectric material was achieved with 1.5 cst silicone oil.

The results establish that pyroelectric energy conversion has great promise. New devices with shorter lengths and lower viscosity working fluids should be experimentally built and tested to validate the trends observed in this paper. Future numerical work should focus on more systematic optimization currently made difficult by the duration of a single simulation lasting 5–7 days.

Acknowledgements

This work was funded in part by the Office of Naval Research under Award N000140710671 (Program Manager: Dr. Mark Spec-

tor). The authors would like to thank Dr. R.B. Olsen for useful discussions and exchange of information.

References

- [1] Lawrence Livermore National Lab, U.S. energy flow trends – 2002, April 16, 2008. Available from: <<http://eed.llnl.gov/flow>>.
- [2] B.T. Liu, K.H. Chien, C.C. Wang, Effect of working fluids on organic Rankine cycle for waste heat recovery, *Energy* 29 (8) (2004) 1207–1217.
- [3] D.G. Thombare, S.K. Verma, Technological development in the Stirling cycle engines, *Renew. Sustainable Energy Rev.* 12 (2008) 1–38.
- [4] S.B. Riffat, X. Ma, Thermoelectrics: a review of present and potential applications, *Appl. Therm. Eng.* 23 (2003) 913–935.
- [5] R.B. Olsen, D.A. Bruno, J.M. Briscoe, W.F. Butler, A pyroelectric energy converter which employs regeneration, *Ferroelectrics* 38 (1981) 975–978.
- [6] R.B. Olsen, Ferroelectric conversion of heat to electrical energy – a demonstration, *J. Energy* 6 (1982) 91–95.
- [7] R.B. Olsen, D.D. Brown, High-efficiency direct conversion of heat to electrical energy related pyroelectric measurements, *Ferroelectrics* 40 (1982) 17–27.
- [8] R.B. Olsen, D.A. Bruno, J.M. Briscoe, Cascaded pyroelectric energy converter, *Ferroelectrics* 59 (1984) 205–219.
- [9] R.B. Olsen, D.A. Bruno, J.M. Briscoe, Pyroelectric conversion cycles, *J. Appl. Phys.* 58 (1985) 4709–4716.
- [10] R.B. Olsen, D.A. Bruno, J.M. Briscoe, Pyroelectric conversion cycle of vinylidene fluoride-trifluoroethylene co-polymer, *J. Appl. Phys.* 57 (1985) 5036–5042.
- [11] R.B. Olsen, D.A. Bruno, Pyroelectric conversion materials, in: Proceedings of the 21st Intersociety Energy Conversion Engineering Conference, American Chemical Society, San Diego, California, August 25–29 1986, pp. 89–93.
- [12] M. Ikura, Conversion of low-grade heat to electricity using pyroelectric copolymer, *Ferroelectrics* 267 (2002) 403–408.
- [13] L. Kouchachvili, M. Ikura, High performance pyroelectric converter, in: Proceedings of the 6th IASTED International Conference European Power and Energy Systems, Rhodes, Greece, June 26–28 2006, pp. 366–371.
- [14] L. Kouchachvili, M. Ikura, Improving the efficiency of pyroelectric conversion, *Int. J. Energy Res.* 32 (2008) 328–335.
- [15] G. Sebald, S. Pruvost, D. Guyomar, Energy harvesting based on Ericsson pyroelectric cycles in a relaxor ferroelectric ceramic, *Smart Mater. Struct.* 17 (2008) 1–6.
- [16] D. Guyomar, S. Pruvost, G. Sebald, Energy harvesting based on FE–FE transition in ferroelectric single crystals, *IEEE Trans. Ultrason. Ferroelectr. Freq. Control* 55 (2008) 279–285.
- [17] A. Khodayari, S. Pruvost, G. Sebald, D. Guyomar, S. Mohammadi, Nonlinear pyroelectric energy harvesting from relaxor single crystals, *IEEE Trans. Ultrason. Ferroelectr. Freq. Control* 56 (2009) 693–699.
- [18] H. Nguyen, A. Navid, L. Pilon, Pyroelectric energy converter using co-polymer P(VDF-TrFE) and Olsen cycle for waste heat energy harvesting, *Appl. Thermal Eng.*, 2010, under review.
- [19] S.B. Lang, Pyroelectricity: from ancient curiosity to modern imaging tool, *Physics Today* 58 (2005) 31–36.
- [20] A.S. Mischenko, Q. Zhang, J.F. Scott, R.W. Whatmore, N.D. Mathur, Giant electrocaloric effect in thin-film $\text{PbZr}_{0.95}\text{Ti}_{0.05}\text{O}_3$, *Science* 311 (2006) 1270–1271.
- [21] A.S. Mischenko, Q. Zhang, R.W. Whatmore, J.F. Scott, N.D. Mathur, Giant electrocaloric effect in the thin film relaxor ferroelectric $0.9\text{PbMg}_{1/3}\text{Nb}_{2/3}\text{O}_3-0.1\text{PbTiO}_3$ near room temperature, *Appl. Phys. Lett.* 89 (2006) 242912.
- [22] T.M. Correia, J.S. Young, R.W. Whatmore, J.F. Scott, N.D. Mathur, Q. Zhang, Investigation of the electrocaloric effect in a $\text{PbMg}_{2/3}\text{Nb}_{1/3}\text{O}_3-\text{PbTiO}_3$ relaxor thin film, *Appl. Phys. Lett.* 95 (2009) 182904.
- [23] B. Neese, S.G. Lu, B. Chu, Q.M. Zhang, Electrocaloric effect of the relaxor ferroelectric poly(vinylidene fluoride-trifluoroethylene-chlorofluoroethylene) terpolymer, *Appl. Phys. Lett.* 94 (2009) 042910.
- [24] R.B. Olsen, W.F. Butler, J.E. Drummond, D.A. Bruno, J.M. Briscoe, Heat flow in a pyroelectric converter, in: 20th Intersociety Energy Conservation Engineering Conference, Miami Beach, Florida 3, November 17–22 1985, pp. 595–602.
- [25] J.A. Gonzalo, Ferroelectric materials as energy converters, *Ferroelectrics* 11 (1976) 423–430.
- [26] A. van der Ziel, Solar power generation with the pyroelectric effect, *J. Appl. Phys.* 45 (1974) 4128.
- [27] D. Vanderpool, J.H. Yoon, L. Pilon, Simulations of a prototypical device using pyroelectric materials for harvesting waste heat, *Int. J. Heat Mass Transfer* 51 (2008) 5052–5062.
- [28] A. Navid, C.S. Lynch, L. Pilon, Purified and porous poly(vinylidene fluoride-trifluoroethylene) [P(VDF-TrFE)] thin films for pyroelectric infrared sensing and energy harvesting, *Smart Mater. Struct.* 19 (2010) 055006.
- [29] Dow Corning Corp., Dow Corning 200® Fluid, 50 and 1.5 cst Product Information Sheet, May 20 2009. Available from: <<http://www.dowcorning.com/applications/search/default.aspx?Ne=4294963250&N=4294963212&hbc=1&DCCD=PRODUCT&WT.svl=1&DCCD=PRODUCT>>.
- [30] C.B. Sawyer, C.H. Tower, Rochelle salt as a dielectric, *Phys. Rev.* 35 (1930) 269–275.
- [31] M.O. Çarpınlioğlu, M.Y. Gündoğdu, A critical review on pulsate pipe flow studies directing towards future research topics, *Flow Meas. Instrum.* 12 (2001) 163–174.
- [32] A. Bejan, *Convection Heat Transfer*, John Wiley and Sons, New York, NY, 2004.

- [33] F.P. Incropera, D.P. DeWitt, *Heat and Mass Transfer*, John Wiley and Sons, Ltd., New York, NY, 2002.
- [34] PI Ceramic, Piezoceramic materials data sheet, March 28 2007.
- [35] R.B. Olsen, D. Evans, Pyroelectric energy conversion: hysteresis loss and temperature sensitivity of a ferroelectric material, *J. Appl. Phys.* 54 (1983) 5941–5944.
- [36] N. Ozawa, M. Shinoki, K. Nagoshi, E. Serizawa, Scaling of heat transfer characteristics in an oscillating flow, *J. Enhanced Heat Transfer* 10 (2003) 275–285.
- [37] H.B. Atabek, C.C. Chang, Oscillatory flow near the entry of a circular tube, *Z. Angew. Math. Phys.* 12 (1961) 185–201.
- [38] X. Niu, J. Yu, S. Wang, Experimental study on low-temperature waste heat thermoelectric generator, *J. Power Sources* 188 (2) (2009) 621–626.